



Article

A Novel Dynamic Li-Ion Battery Model for the Aggregated Charging of EVs

Ahmed M. Asim^{1,*}, Osama A. Ahmed², Amr M. Ibrahim¹ , Walid Aly El-Khattam¹ and Hossam E. Talaat^{3,*}

¹ Department of Electrical Power and Machines Engineering, University of Ain Shams, Cairo 11566, Egypt; amr_rizk@eng.asu.edu.eg (A.M.I.); walid.elkhattam@eng.asu.edu.eg (W.A.E.-K.)

² Department of Electrical Engineering, University of Tabuk, Tabuk 71491, Saudi Arabia

³ Department of Electrical Engineering, Future University in Egypt, Cairo 11835, Egypt

* Correspondence: ahmedasimasu@eng.asu.edu.eg (A.M.A.); hossam.eldeen@fue.edu.eg (H.E.T.)

Abstract: Implementing successful aggregated charging strategies for electric vehicles to participate in the wholesale market requires an accurate battery model that can operate at scale while capturing critical battery dynamics. Existing models either lack precision or pose computational challenges for fleet-level coordination. To our knowledge, most of the literature widely adopts battery models that neglect critical battery polarization dynamics favoring scalability over accuracy, donated as constant power models (CPMs). Thus, this paper proposes a novel linear battery model (LBM) intended specifically for use in aggregated charging strategies. The LBM considers battery dynamics through a linear representation, addressing the limitations of existing models while maintaining scalability. The model dynamic behavior is evaluated for the four commonly used lithium-ion chemistries in EVs: lithium iron phosphate (LFP), nickel manganese cobalt (NMC), lithium manganese oxide (LMO), and nickel cobalt aluminum (NCA). The results showed that the LBM closely matches the high-fidelity Thevenin equivalent circuit model (Th-ECM) with substantially improved accuracy over the CPM, especially at higher charging rates. Finally, a case study was carried out for bidding in the wholesale energy market, which proves the ability of the model to scale.

Keywords: lithium-ion battery; aggregator; aggregation; equivalent circuit model; battery modeling; electric vehicles; fleet management; linear model; V2G



Citation: Asim, A.M.; Ahmed, O.A.; Ibrahim, A.M.; El-Khattam, W.A.; Talaat, H.E. A Novel Dynamic Li-Ion Battery Model for the Aggregated Charging of EVs. *World Electr. Veh. J.* **2023**, *14*, 336. <https://doi.org/10.3390/wevj14120336>

Academic Editor: Zhaoyun Zhang

Received: 28 October 2023

Revised: 21 November 2023

Accepted: 28 November 2023

Published: 4 December 2023



Copyright: © 2023 by the authors. Licensee MDPI, Basel, Switzerland. This article is an open access article distributed under the terms and conditions of the Creative Commons Attribution (CC BY) license (<https://creativecommons.org/licenses/by/4.0/>).

1. Introduction

Electric vehicles have gained momentum as a sustainable and eco-friendly alternative to traditional internal combustion engine vehicles [1–3]. Their widespread adoption has been driven by various factors, including environmental consciousness, government incentives, and advances in battery technology. Importantly, EVs possess a unique capability to address the issue of renewable energy intermittency [4,5]. When connected to a grid, EVs can serve as mobile energy storage units, acting as a buffer to absorb excess energy during periods of high electricity production and release it during low-production or peak demand periods [6]. This bidirectional energy flow, facilitated by intelligent vehicle-to-grid (V2G) systems, contributes to more balanced and stable grid operation [7].

The electric vehicle energy conversion chain starts with the grid charging power being conditioned through rectifiers and converters to charge the battery packs [8]. The stored chemical energy is then converted to electrical energy through the battery's internal reactions during discharge. This electrical energy flows through inverters, converters, and motors to provide mechanical motion energy to the wheels for propelling the vehicle. Along this conversion process, the battery management system (BMS) provides monitoring and control functions, including estimating the State of Charge (SoC) and State of Health (SoH) parameters for the controlled battery pack [9]. Among the various types of batteries available for EVs, Li-ion batteries have emerged as the

predominant choice [10,11]. They excel compared to other battery chemistries due to their high energy density, longer cycle life, fast charging capabilities, lower self-discharge rate, lightweight design, efficiency, suitability for regenerative braking, and comparatively reduced environmental impact [12,13]. The ability of lithium-ion batteries to efficiently store and deliver energy renders them well-suited for V2G applications, enhancing EVs' potential to address renewable intermittency [14].

EV smart-scheduled charging can reduce peak demand, ultimately enhancing distribution network stability and lowering operating and upgrading costs for utility companies [15]. Moreover, the coordinated charging and discharging of EVs can act as a valuable grid resource capable of smoothing out fluctuations in supply and demand, storing excess energy during periods of surplus, and then injecting it back into the grid during peak demand [16,17]. Thus, collective smart fleet charging and discharging platforms (in short fleet charging platforms) have the potential to transform EVs from simple consumers of electricity to dynamic energy storage and grid support assets.

According to [18], fleet charging platforms face multiple complex challenges in managing a large number of EVs while interacting with the power grid. Recent research efforts have aimed to address each of these challenges through advanced algorithms, robust optimization techniques, pricing incentives, and stakeholder coordination. Specifically, the uncertainty in EV owner behavior, like arrival and departure times, poses difficulties in optimizing fleet charging schedules. Stochastic programming and robust optimization methods have been proposed to deal with these uncertain parameters [19]. On the computational complexity side, decomposition techniques and distributed algorithms are being applied to break down large fleet optimization problems into more manageable sub-problems [20]. To account for EV battery degradation, models have incorporated degradation costs into scheduling objectives and constraints [21]. Approaches like stochastic programming and conditional value-at-risk methods have also emerged to manage the risks of market participation [22]. For coordination needs, decentralized and agent-based solutions allow EV aggregators and stakeholders to interact productively [23]. Infrastructure planning for charging stations now factors in aggregator operations and uses advanced metaheuristics [24]. Regarding regulations, recent policy analyses have helped to value grid services properly and avoid issues, such as deviation penalties and market exclusion [25]. Lastly, for customer engagement, pricing incentives and behavioral models are being developed to influence charging patterns [26].

The aforementioned research efforts tackle many challenges. However, many aspects still need further attention, refinements, and research [18,27]. One of these aspects is to improve the accuracy of models used in fleet charging platforms to minimize market participation risks and the uncertainty of the whole process. Thus, it is fundamental for modern fleet charging platforms to implement advanced battery models that are accurate and can be scaled. Thevenin equivalent circuit models (Th-ECMs), which are commonly used in battery management systems (BMSs), are an accurate description of battery dynamics [28]. However, utilizing Th-ECMs with large numbers of vehicles has two scalability challenges: (a) not being linear in terms of power and energy while fleet charging platforms deal with them, and (b) relying on lookup tables for monitoring the state of charge and open circuit voltage [29]. These challenges lead to the wide adoption of what we call the battery constant power model (CPM) [30–34], which neglects all battery polarization dynamics that may lead to a mismatch between the expectations of fleet charging platforms and the reported values from the BMSs. The aim of this research was to develop a dynamic model for Li-ion batteries that narrows down this mismatch without adding many computational requirements and which improves the fleet charging platform's insights and decision accuracy.

This paper is structured as follows: Section two summarizes Li-ion battery models, focusing on Th-ECM and CPM, while the proposed model is developed in Section three. In Section four, a detailed comparative analysis between the proposed model, Th-ECM, and CPM is conducted for the commonly used Li-ion battery chemistries in EVs. Finally, Section five provides a concise conclusion summarizing the key findings of this paper. For convenience, the definitions for the abbreviations and symbols used in this paper are provided in Abbreviations.

2. Li-Ion Battery Models

Modeling batteries using equivalent electrical circuits is widely used since it focuses on describing the battery's electrical behavior. The Randles circuit, Figure 1, accurately models the electrochemical behavior of Li-ion batteries [35].

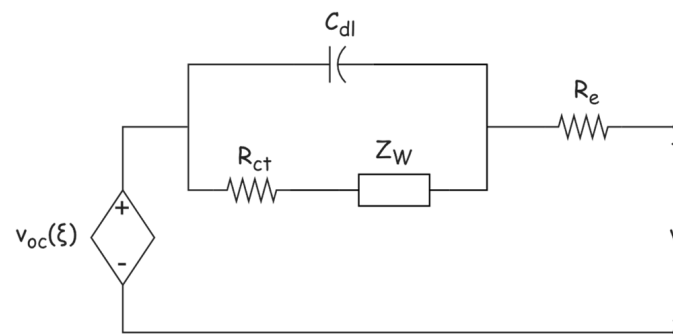


Figure 1. Randles equivalent circuit.

R_e is the electrolyte resistance, R_{ct} is the charge transfer resistance that considers the loading voltage drop voltage over the electrode–electrolyte interface, C_{dl} is the double-layer capacitance modeling the effect of charges building up in the electrolyte at the electrode surface, and the Warburg impedance, Z_W , models the diffusion of lithium ions in the electrodes. Modeling Z_W is challenging due to its frequency-dependent characteristics. Z_W is modeled as infinitely series-connected RC branches [36], as shown in Figure 2.

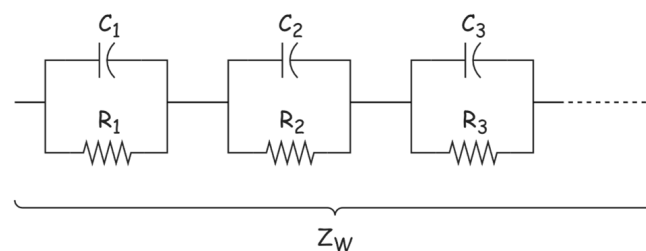


Figure 2. Warburg impedance RC branches equivalence.

The state of charge (ξ) dependent voltage source (v_{oc}) represents the battery open circuit voltage. This dependency is usually modeled as a lookup table, which depends on the battery chemistry [29]. Figure 3 shows v_{oc} against ξ for each of the commonly used types in EVs: lithium iron phosphate (LFP), nickel manganese cobalt (NMC), lithium manganese oxide (LMO), and nickel cobalt aluminum (NCA) [37].

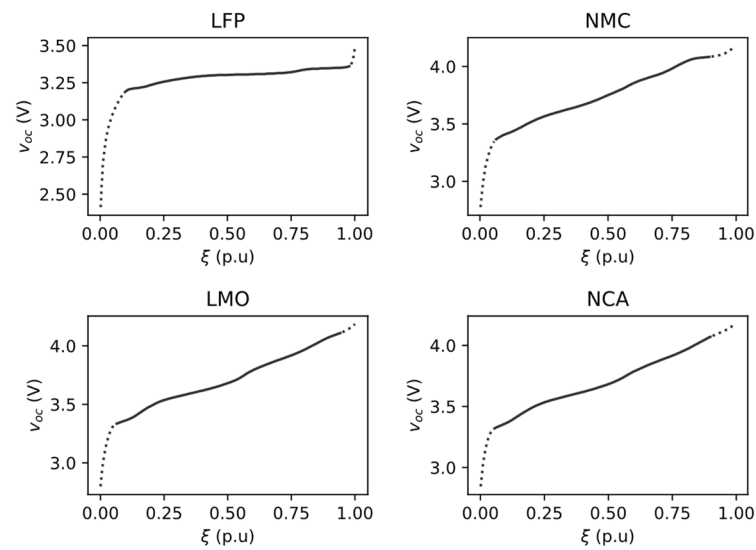


Figure 3. Open circuit voltage for various battery chemistries. The solid portions represent the practical operational regions.

2.1. Thevenin Equivalent Circuit Model (Th-ECM)

Figure 4 shows the Thevenin equivalent circuit model (Th-ECM), which is the most widely used approximation of Randles circuit in which the Warburg impedance is approximated by a finite number, N (usually one to three branches are used) of RC branches [36], the usually negligible double layer capacitance, C_{dl} is omitted, and the charge transfer resistance, R_{ct} , and the electrolyte resistance, R_e , are joined into a single resistance, R_0 .

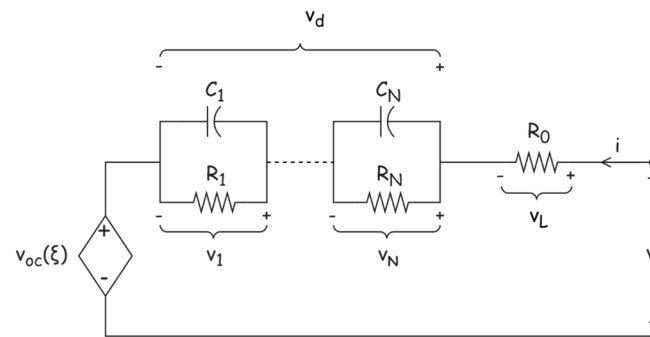


Figure 4. Li-ion battery Thevenin equivalent circuit.

According to Th-ECM, battery terminal voltage, v , is polarized from v_{oc} by the diffusion voltage, $v_d = \sum_n v_n$, and the loading voltage drop, $v_l = R_0 i$ as in:

$$v = v_{oc}(\xi) + \sum_n v_n + R_0 i \tag{1}$$

where v_n , is the n^{th} RC branch voltage, and i is the battery terminal current. Note that the charging current is adopted as positive.

Since v_{oc} is ξ dependent, tracking ξ is required. The value of ξ can be updated at each time step by using the following equation:

$$\xi[k + 1] = \xi[k] + \frac{\eta_c T_s}{Q} i[k] \tag{2}$$

where η_c is the battery coulombic efficiency, Q is the battery coulombic capacity, and T_s is the sampling period.

The use of multiple RC circuits was studied in [38], such that the voltage of each branch is described using the differential equation $\dot{v}_n = -v_n/R_nC_n - R_ni/R_nC_n$. Using zero-order hold discretization, v_n state transition could be expressed as:

$$v_n[k+1] = e^{-T_s/\tau_n} v_n[k] + (1 - e^{-T_s/\tau_n}) R_n i[k] \quad (3)$$

where R_n , C_n , and τ_n are the n^{th} RC branch resistance, capacitance, and time constant, respectively.

Additionally, chargers must adhere to strict operational voltage and current limits to avoid rapid battery degradation [39,40].

$$V_{\min} \leq v \leq V_{\max} \quad (4)$$

$$-I_{\text{dis,max}} \leq i \leq I_{\text{chg,max}} \quad (5)$$

where V_{\min} and V_{\max} are the battery operational voltage limits, and $I_{\text{chg,max}}$ and $I_{\text{dis,max}}$ are the charging and discharging operational current limits, respectively. The solid region denotes the voltage limits in Figure 3.

To our knowledge, Th-ECM is the most widely used model in modern battery management systems (BMSs) [28]. Th-ECM clearly states (2) and (3) as state transition equations with i as an input variable and ζ and v_n as state variables. These state variables are used to inherently observe v_{oc} via the lookup table while explicitly observing v using the output Equation (1). The integration of Th-ECM with fleet charging platforms requires observing, for every vehicle, stored energy (E) and terminal power (p) with:

$$E[k+1] = E[k] + v_{oc}[k]i[k]T_s \quad (6)$$

$$p[k] = i[k]v[k] \quad (7)$$

In terms of the E and p observables, the model is nonlinear with an increased number of variables and a lookup table for v_{oc} [29]. This computationally limits the scalability of the model to a large number of EVs. Thus, researchers used simplified battery models to integrate with their developed fleet charging platforms with wide dominance of what we call the constant power model (CPM).

2.2. Constant Power Model (CPM)

The CPM is a simple model that only considers the dynamics in stored energy with a single state transition equation:

$$E[k+1] = E[k] + \eta_e p[k]T_s \quad (8)$$

where η_e is the battery energy efficiency.

Note that in this model, E is the only state variable with p as a single input variable. The major assumption used by the CPM is considering the E and p variables to have constant bounds [32] as:

$$-P_{\text{dis,max}} \leq p[k] \leq P_{\text{chg,max}} \quad (9)$$

$$E_{\min} \leq E[k] \leq E_{\max} \quad (10)$$

where $P_{\text{chg,max}}$ and $P_{\text{dis,max}}$ are the charging and discharging operational power limits, and E_{\min} and E_{\max} are the battery operational energy limits.

Since power limits are not constant, $P_{\text{dis,max}}$, and $P_{\text{chg,max}}$ are average values that could be calculated as:

$$P_{\text{dis,max}} = \frac{1}{2}(V_{\min}I_{\text{dis,max}} + V_{\max}I_{\text{dis,max}}) \quad (11)$$

$$P_{\text{chrg,max}} = \frac{1}{2} (V_{\text{min}} I_{\text{chrg,max}} + V_{\text{max}} I_{\text{chrg,max}}) \quad (12)$$

Comparing the two models, the CPM ignores all polarization dynamics and the effect of open circuit voltage variation with the SoC and assumes constant energy efficiency independent of the charging current [32]. These neglects of the CPM lead to a considerable mismatch between fleet charging platform expectations and the reported values using BMSs. For instance, by considering only the loading polarization effect for charging at the maximum rate of 1C, a 3.2 Ah NCA battery with the parameters $V_{\text{min}} = 3.3$ V, $V_{\text{max}} = 4.2$ V and a total internal resistance of 0.098Ω exists [37]. Then, if $v_{oc} = 4$ V, the BMS would report a maximum charging power of 8.57 W according to (1) and (7) without breaking the operational voltage limits, while for the CPM according to (12), the maximum charging power is 12 W regardless of the current SoC or open circuit voltage. This shows the need for developing a battery model that narrows down this mismatch without adding many computational requirements, which improves the fleet charging platform's insights and decision accuracy.

3. Proposed Linear Battery Model (LBM)

Instead of adding more observables to the Th-ECM to track E and p , the developed model is a set of transformations and approximations applied to Th-ECM, mapping it to the power/energy domain.

3.1. Voltage Transformation

When a Li-ion battery is fully charged, its OCV is at its highest, indicating substantial stored energy, and when it is empty, its OCV is at its lowest, indicating depleted stored energy. This provides a glimpse of an intrinsic relation (transformation) between v_{oc} and E .

For instance, a small charge injection of dq changes the battery state of charge by $d\zeta = \eta_c dq/Q$ and the battery stored energy by $dE = v_{oc}(\zeta)\eta_c dq$. Then, dE could be stated in terms of $d\zeta$ as:

$$dE = Qv_{oc}(\zeta)d\zeta \quad (13)$$

By integrating dE , the value of stored energy, E , at any ζ could be expressed as:

$$E(\zeta) = Q \int_0^{\zeta} v_{oc}(\zeta') d\zeta' \quad (14)$$

Equation (14) indirectly proves that there is one-to-one transformation between E and v_{oc} . For instance, consider two states of charge, ζ_1 and ζ_2 , with corresponding stored energies, E_1 and E_2 , and open circuit voltages, v_{oc1} and v_{oc2} , respectively. Then, if $E(\zeta_1) = E(\zeta_2)$, we have:

$$\int_0^{\zeta_1} v_{oc}(\zeta') d\zeta' = \int_0^{\zeta_2} v_{oc}(\zeta') d\zeta' \quad (15)$$

Both integrals start from zero, and $v_{oc}(\zeta)$ is monotonic with ζ , as shown in Figure 3, therefore ζ_1 must equal ζ_2 . If two definite integrals of an increasing function are equal $\int_a^{b_1} f(x)dx = \int_a^{b_2} f(x)dx$, then it implies that b_1 must equal b_2 , as assuming otherwise leads to a contradiction, since the difference between the integrals $\int_{b_1}^{b_2} f(x)dx$ is greater than zero due to the function's monotonicity. Figure 3 also shows that if $\zeta_1 = \zeta_2$, then v_{oc1} should equal v_{oc2} . This proves that ζ , v_{oc} , and E have bijective relationships; knowing one of them provides all the information needed to observe the others.

To visualize the bijective relationship between v_{oc} and E , the stored energy is calculated for each ζ according to (14), then plotted against the corresponding v_{oc} as shown in Figure 5, with the solid portions of the curves representing the practical operational region.

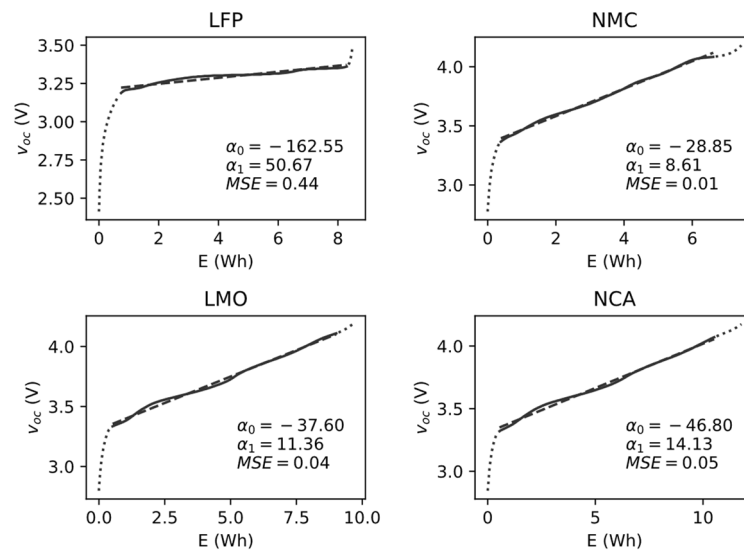


Figure 5. Stored energy vs. voltage.

Surprisingly, these figures depict curves that very closely resemble linearity within the practical operational range for the four commonly used Li-ion battery types. This suggests the approximation of the relationship between v_{oc} and energy as a straight line, expressed as:

$$E = \alpha_0 + \alpha_1 v_{oc} \tag{16}$$

Achieving a linear one-to-one correspondence between v_{oc} and E that is independent of the history or the present and past currents greatly simplifies the model and removes the model's dependency on lookup tables.

Equation (16) could be interpreted as a transformation between the voltage and energy. If the same transformation is applied to the terminal voltage, v , as in (17), a new energy term is introduced, denoted as E_a , which stands for the apparent energy.

$$E_a = \alpha_0 + \alpha_1 v \tag{17}$$

Then, v operational limits could be described in terms of E_a using the following equation:

$$E_{\min} \leq E_a \leq E_{\max} \tag{18}$$

where $E_{\min} = \alpha_0 + \alpha_1 V_{\min}$ and $E_{\max} = \alpha_0 + \alpha_1 V_{\max}$ are the battery operational energy limits.

Equations (16) and (17) describe the analogy between voltages and energies. For instance, during the battery charging process, v deviates from v_{oc} and it is crucial to ensure that v should not exceed V_{\max} . Once v reaches V_{\max} , the battery appears as if it fully charged. Similarly, E_a deviates from E and it is crucial to ensure that E_a should not exceed E_{\max} . Hitting E_{\max} causes the battery to appear as if it is fully charged. This comparison highlights the analogy between E_a and v .

To describe the relation between E_a and E , Equations (16) and (17) are substituted in (1), and results in $E_a = E + \sum_n \alpha_1 v_n + R_0 \alpha_1 i$. This shows that E_a is deviated from E by the loading energy deviation $R_0 \alpha_1 i$ and diffusion energy deviation $\sum_n \alpha_1 v_n$. Then, by introducing $E_n = \alpha_1 v_n$ as the deviation in energy due to n^{th} RC branch, Equations (1) and (3) could be restated in terms of energies and current by the following equation:

$$E_a = E + \sum_n E_n + R_0 \alpha_1 i \tag{19}$$

$$E_n[k + 1] = e^{-T_s/\tau_n} E_n[k] + \left(e^{-T_s/\tau_n} - 1 \right) R_n \alpha_1 i[k] \tag{20}$$

3.2. Current Transformation

Up to this point, the model uses i as the input variable, while the fleet charging platforms control terminal power instead. Fortunately, the operational current limits could be stated in terms of p and E_a without approximation. This can be achieved by multiplying all sides of (5) by v , then substituting vi with p and v with $(E_a - \alpha_0)/\alpha_1$, resulting in:

$$-I_{\text{dis,max}} \left(\frac{E_a - \alpha_0}{\alpha_1} \right) \leq p \leq I_{\text{chg,max}} \left(\frac{E_a - \alpha_0}{\alpha_1} \right) \quad (21)$$

Since E and ξ are proven to be bijective, then (6) could be used as a state transition equation instead of (2), which could be stated in terms of E and P as:

$$E[k+1] = E[k] + \frac{v_{oc}[k]}{v[k]} p[k] T_s \quad (22)$$

To linearize this equation, the ratio v_{oc}/v could be approximated using a constant value α_r . Then, the linear form of (18) is:

$$E[k+1] = E[k] + \alpha_r p[k] T_s \quad (23)$$

Notably, v_{oc}/v is less than the unity during charging, while it exceeds the unity during discharging. In steady-state conditions, capacitors are open circuit, thus, this ratio could be expressed as:

$$\frac{v_{oc}}{v} = \frac{1}{1 + \frac{(R_0 + \sum_n R_n)i}{v_{oc}}} \quad (24)$$

α_r is defined as the average of v_{oc}/v . Then, to find the precise value for α_r , the joint probability distribution between v_{oc} and i should be studied. However, in this work α_r is simply estimated as:

$$\alpha_r = \frac{\left(\frac{v_{oc}}{v}\right)_{\text{max}} + \left(\frac{v_{oc}}{v}\right)_{\text{min}}}{2} \quad (25)$$

These maximum and minimum values of v_{oc}/v could be obtained by optimizing (24) while subjected to (5) and:

$$V_{\text{min}} \leq v_{oc} + \left(R_0 + \sum_n R_n \right) i \leq V_{\text{max}} \quad (26)$$

where the term $v_{oc} + (R_0 + \sum_n R_n)i$ is the steady-state terminal voltage.

Equations (19) and (20) could be rewritten in terms of power as:

$$E_a = E + \sum_n E_n + R_0 \alpha_1 \frac{p}{v} \quad (27)$$

$$E_n[k+1] = e^{-T_s/\tau_n} E_n[k] + \left(e^{-T_s/\tau_n} - 1 \right) R_n \alpha_1 \frac{p[k]}{v[k]} \quad (28)$$

To linearize both equations, the term $1/v$ could be approximated to the constant value α_v . Then, the (27) and (28) linear representations are:

$$E_a = E + \sum_n E_n + R_0 \alpha_1 \alpha_v p \quad (29)$$

$$E_n[k+1] = e^{-T_s/\tau_n} E_n[k] + \left(1 - e^{-T_s/\tau_n} \right) R_n \alpha_1 \alpha_v p[k] \quad (30)$$

α_v is defined as the average of $1/v$. To find the precise value for α_v , the probability distribution of v should be studied. However, in this work α_v is simply estimated as:

$$\alpha_v = \frac{1}{2} \left(\frac{1}{V_{\min}} + \frac{1}{V_{\max}} \right) \tag{31}$$

The validity of using the average values for the ratio v/v_{oc} and $1/v$, could be proven by comparing the overall performance of the proposed model with Th-ECM, which is conducted in the next section.

4. Developed Battery Model Evaluation

A comparative analysis was conducted between the dynamics of the LBM and CPM against Th-ECM, for the LFP, NMC, LMO, and NCA batteries. Battery data were obtained from [37] and listed in Table 1. For the LBM, the linear fit parameters α_0 and α_1 for each battery were estimated as described in Section 2.1. Then, α_r and α_v were estimated according to (25) and (31). For the CPM, the values of $P_{\text{dis,max}}$ and $P_{\text{chr,max}}$ were calculated by using (11) and (12), respectively.

Table 1. Battery parameters.

	LFP	NMC	LMO	NCA
Q	2.6 Ah	2 Ah	2.6 Ah	3.2 Ah
R_0	0.0291 Ω	0.0618 Ω	0.0440 Ω	0.1082 Ω
R_1	0.0394 Ω	0.0366 Ω	0.0422 Ω	0.0469 Ω
C_1	634.1 F	1110.1 F	1067.3 F	1072.2 F

4.1. Accuracy Evaluation of the Charging and Discharging Dynamics of the LBM

The charging and discharging simulations were performed using Google Colab by optimizing the AMPL models with a BONMIN solver. All batteries were simulated for full charge-discharge cycles. The charging dynamics, in terms of both the energy and power at a rate of 1C, are visualized in Figure 6, while the discharging dynamics are presented in Figure 7. The curves show that the LBM closely approximates the Th-ECM, whereas the CPM has a notable mismatch.

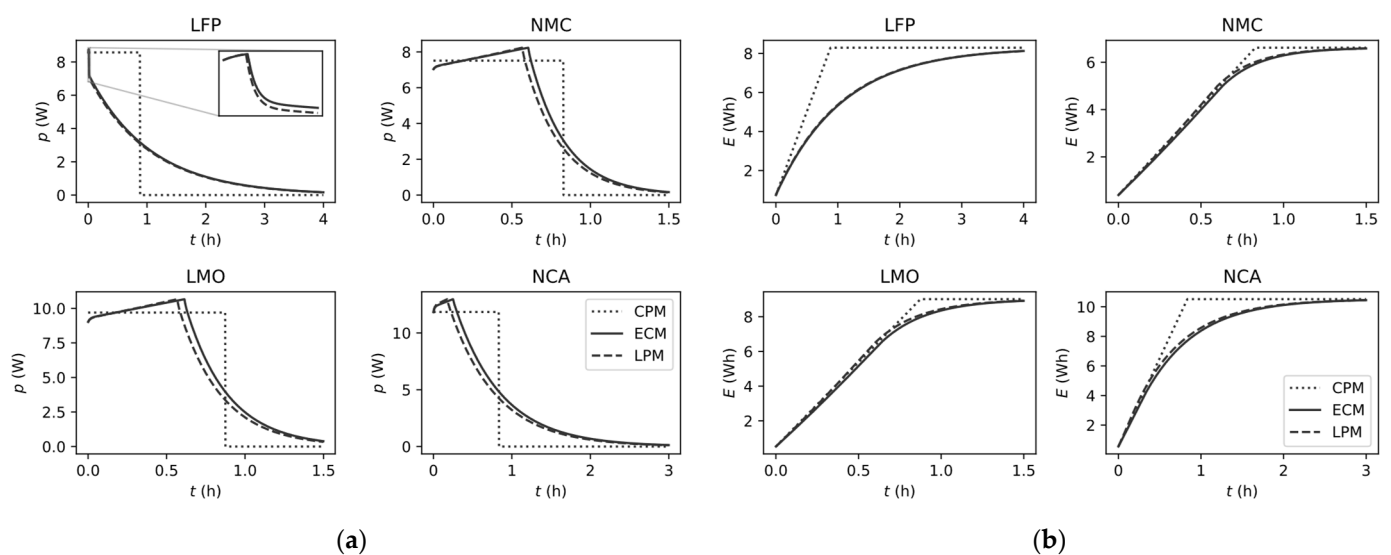


Figure 6. The charging dynamics at a rate of 1C for the LFP, NMC, LMO, and NCA batteries: (a) terminal power dynamics; (b) stored energy dynamics.

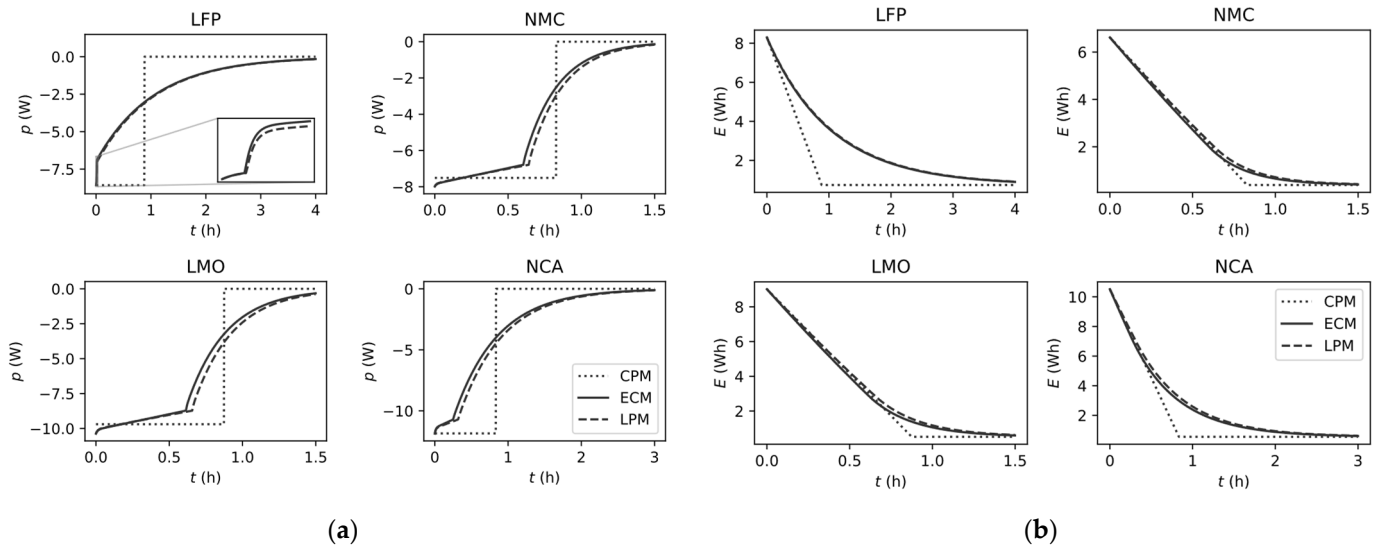


Figure 7. Discharging dynamics at a rate of 1C rate for the LFP, NMC, LMO, and NCA batteries: (a) terminal power dynamics; (b) stored energy dynamics.

For the power dynamics depicted in Figures 6a and 7a, both the Th-ECM and LBM demonstrate a noticeable inflection point, signifying the transition from the constant current (CC) to the constant voltage (CV) phase. In contrast, in the CPM, the power transition indicates the end of the charging or discharging process. These deviations are more pronounced in batteries that have shorter periods of constant current (CC), such as those using lithium iron phosphate (LFP) chemistry and nickel cobalt aluminum oxide (NCA) batteries. These shorter CC phases occur because LFP has a limited voltage range, and NCA batteries have a high R_0 value of 0.1082 Ω .

The noticeable difference in the power behavior between the CPM and Th-ECM leads to significant variations in energy patterns, as shown in Figures 6b and 7b. These differences, especially near full charge, lead to a huge mismatch between the expectations of the fleet charging platforms and the reported values from the BMS. This difference may cause the fleet management system to continuously readopt to the newly reported values, adding more computational burden.

One of the most significant trends in EV charging is the move towards faster charging speeds, which in turn requires batteries to handle higher C rates [41]. For instance, Figure 8, shows the power and energy dynamics during batteries being charged at an accelerated rate of 1.5C. It is worth noting that, in comparison to the 1C, the duration of the constant current (CC) phases notably contracts, leading to a higher discrepancy between the CPM and ECM responses.

4.2. The Scalability of the LBM Compared to the ECM and CPM

To compare the scalability of the three models, a low computational overhead fleet participation model in the wholesale energy market was utilized. This simple model was formulated as:

$$\min \sum_j \sum_k p_j[k] \cdot T_s \cdot C_k \tag{32}$$

Subjected to:

$$E_j[k_j^{\text{arr}}] = E_j^{\text{arr}} \tag{33}$$

$$E_j[k_j^{\text{dep}}] \geq E_j^{\text{dep}} \tag{34}$$

where j is the electric vehicle index and ranges from 1 to s , s is the fleet size, C_k is the forecasted day-ahead cost of energy at instant k , k_j^{arr} and k_j^{dep} are the arrival and departure instants, and E_j^{arr} and E_j^{dep} are charged to E_j .

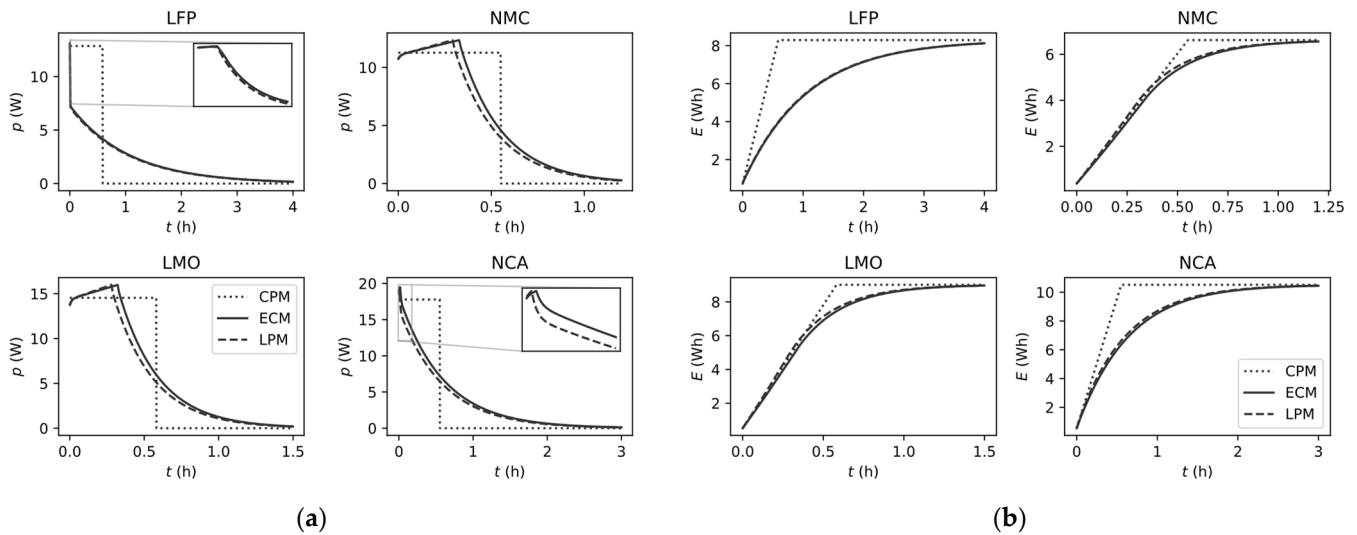


Figure 8. Discharging dynamics at a rate of 2C for LFP, NMC, LMO, and NCA batteries: (a) terminal power dynamics; (b) stored energy dynamics.

To understand how well the ECM, LPM, and CPM scale, we optimized the market participation model for different scenarios of fleet sizes and battery models, employing the BONMIN solver with consistent Google Colab CPU and RAM configurations. For every scenario, the time to an optimal solution was averaged over five runs. This approach enhances the precision of our measurements. The collective findings are presented in Figure 9, showing the relationship between fleet size (s) and convergence time for the ECM, LBM, and CPM across 4 chemistries: LFP, NMC, LMO, and NCA. The x axis shows the size of the fleet and the y axis shows the time in seconds.

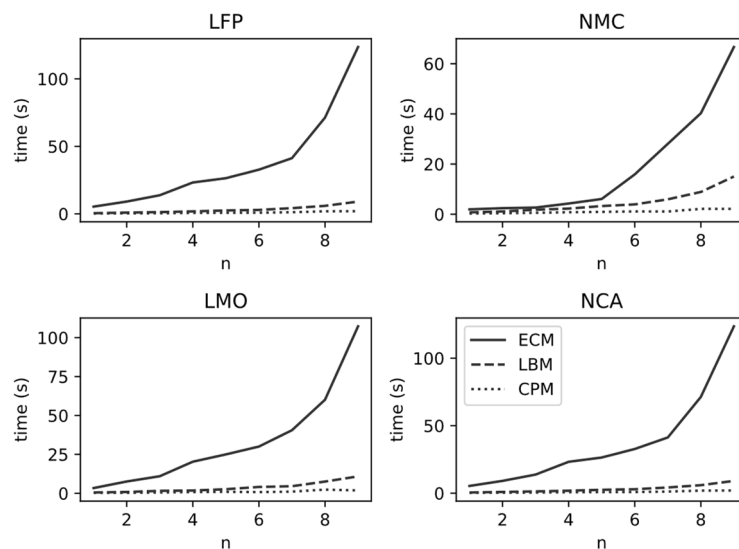


Figure 9. Convergence time in seconds for reaching optimal solutions across a various number of EVs for the LFP, NMC, LMO, and NCA fleets.

The graphs show that, as the number of vehicles increases, the time taken to reach the optimal solution also increases. The results indicate that convergence times are also dependent on battery chemistry for the Th-ECM and LBM. Notably, NMC and LMO

converge faster than NCA and LFP, which may indicate a correlation between the CC period duration and the computational complexity of the problem. The data suggest that the CPM model is the most scalable, followed by the LBM and Th-ECM, with a noticeable gap. The results of this study proved our claim that the LBM has a better ability to scale than the Th-ECM.

5. Conclusions

In conclusion, this research successfully developed a Li-ion linear battery model (LBM) as a valuable tool for smart fleet charging platforms. The LBM addresses the critical battery polarization dynamics while maintaining scalability through linearity in the power and energy domain. The comparative analysis against the constant power model (CPM) and Thevenin equivalent circuit model (Th-ECM) across various Li-ion battery chemistries demonstrates the LBM's superior accuracy, especially for LFP and NCA chemistries. Notably, the accuracy advantage of the LBM over the CPM is more pronounced at higher charging rates. Moreover, measuring the conversion times for the three models tested on a simple energy market participation problem showed a noticeably large improvement in LBM scalability over Th-ECM. These findings highlight the potential of the LBM to significantly enhance the performance of fleet charging platforms, advancing the integration of electric vehicles into more efficient grid support systems.

Author Contributions: Conceptualization, A.M.A., O.A.A., A.M.I., W.A.E.-K. and H.E.T.; methodology, A.M.A., O.A.A., A.M.I., W.A.E.-K. and H.E.T.; software, A.M.A.; validation, A.M.A., O.A.A., A.M.I., W.A.E.-K. and H.E.T.; formal analysis, A.M.A.; investigation, A.M.A.; writing—original draft preparation, A.M.A.; writing—review and editing, A.M.A. and O.A.A.; visualization, A.M.A.; supervision, O.A.A., A.M.I., W.A.E.-K. and H.E.T.; All authors have read and agreed to the published version of the manuscript.

Funding: The APC was funded by Future University in Egypt.

Data Availability Statement: Data are contained within the article.

Conflicts of Interest: The authors declare no conflict of interest.

Abbreviations

BMS	Battery management system
CC	Constant current
CPM	Constant power model
CV	Constant voltage
EV	Electric vehicle
LBM	Linear battery model
LFP	Lithium iron phosphate
LMO	Lithium manganese oxide
NCA	Nickel cobalt aluminum
NMC	Nickel manganese cobalt
OCV	Open circuit voltage
SoC	State of charge
SoH	State of health
Th-ECM	Thevenin equivalent circuit model
V2G	Vehicle to grid
Indices	
n	Index of RC branches, ranges from 1 to N.
j	Index of EVs inside a fleet, ranges from 1 to s (fleet size)
k	Index of time instant, ranges from 1 to (simulation time)/ T_s

Parameters	
R_e	Electrolyte resistance
R_{ct}	Charge transfer resistance
C_{dl}	Double-layer capacitance
Z_W	Warburg impedance
R_0	Total internal resistance
η_c	Columbic efficiency
Q	Columbic capacity
T_s	Sampling period
R_n	The n^{th} RC branch resistance
C_n	The n^{th} RC branch capacitance
τ_n	The n^{th} RC branch time constant
V_{min}	Minimum operational voltage limit
V_{max}	Maximum operational voltage limit
$I_{dis,max}$	Maximum operational discharging current limit
$I_{chg,max}$	Maximum operational charging current limit
η_e	Energy efficiency
$P_{dis,max}$	Maximum operational discharging power limit
$P_{chg,max}$	Maximum operational charging power limit
E_{min}	Minimum operational energy limit
E_{max}	Maximum operational energy limit
α_0	The zero-order coefficient for linearly fitting E to v_{oc}
α_1	The first-order coefficient for linearly fitting E to v_{oc}
α_r	The mean of v_{oc}/v under typical battery usage pattern
α_v	The mean of $1/v$ under typical battery usage pattern
C_k	The forecasted day-ahead energy cost at instant k
k_j^{arr}/k_j^{dep}	Arrival/departure instant of electric vehicle j
E_j^{arr}/E_j^{dep}	Arrival/departure energy of electric vehicle j
Variables	
ξ	State of charge
v_{oc}	Open circuit voltage
v	Terminal voltage
v_d	Polarization in terminal voltage due to ion diffusion
v_n	Diffusion voltage polarization component of the n^{th} RC branch
v_l	Polarization in terminal voltage due to loading
i	Terminal current
E	Stored energy
p	Terminal power
E_a	Apparent energy
E_n	Polarization in energy due to n^{th} RC branch
p_j	Terminal power for a fleet vehicle with index j
E_j	Stored energy for a fleet vehicle with index j

References

1. Singh, K.V.; Bansal, H.O.; Singh, D. A comprehensive review on hybrid electric vehicles: Architectures and components. *J. Mod. Transp.* **2019**, *27*, 77–107. [\[CrossRef\]](#)
2. Sanguesa, J.A.; Torres-Sanz, V.; Garrido, P.; Martinez, F.J.; Marquez-Barja, J.M. A Review on Electric Vehicles: Technologies and Challenges. *Smart Cities* **2021**, *4*, 372–404. [\[CrossRef\]](#)
3. Costa, C.M.; Carlos, M. Electric vehicles: To what extent are environmentally friendly and cost effective?—Comparative study by european countries. *Renew. Sustain. Energy Rev.* **2021**, *151*, 111548. [\[CrossRef\]](#)
4. Raveendran, V.; Alvarez-Bel, C.; Manjula, G. Assessing the ancillary service potential of electric vehicles to support renewable energy integration in touristic islands: A case study from Balearic island of Menorca. *Renew. Energy* **2020**, *161*, 495–509. [\[CrossRef\]](#)
5. Dik, A.; Omer, S.; Boukhanouf, R. Electric Vehicles: V2G for Rapid, Safe, and Green EV Penetration. *Energies* **2022**, *15*, 803. [\[CrossRef\]](#)
6. Icaza, D.; Borge-Diez, D.; Galindo, S.P.; Flores-Vázquez, C. Analysis of Smart Energy Systems and High Participation of V2G Impact for the Ecuadorian 100% Renewable Energy System by 2050. *Energies* **2023**, *16*, 4045. [\[CrossRef\]](#)
7. Ullah, Z.; Ullah, K.; Diaz-Londono, C.; Grusso, G.; Basit, A. Enhancing Grid Operation with Electric Vehicle Integration in Automatic Generation Control. *Energies* **2023**, *16*, 7118. [\[CrossRef\]](#)

8. Bayati, M.; Abedi, M.; Farahmandrad, M.; Gharehpetian, G.B.; Tehrani, K. Important Technical Considerations in Design of Battery Chargers of Electric Vehicles. *Energies* **2021**, *14*, 5878. [[CrossRef](#)]
9. Gholizadeh, M.; Yazdizadeh, A. SOC and SOH Estimation for a Lithium-Ion Battery Using a Novel Adaptive Observer Based Approach. In Proceedings of the 2020 28th Iranian Conference on Electrical Engineering (ICEE), Tabriz, Iran, 4–6 August 2020; IEEE: Piscataway, NJ, USA, 2020; pp. 1–6.
10. Hannan, M.A. Review of energy storage systems for electric vehicle applications: Issues and challenges. *Renew. Sustain. Energy Rev.* **2017**, *69*, 771–789. [[CrossRef](#)]
11. El Baset Abd El Halim, A.A.; Bayoumi, E.H.E.; El-Khattam, W.; Ibrahim, A.M. Electric Vehicles: A Review of Their Components and Technologies. *Int. J. Power Electron. Drive Syst.* **2022**, *13*, 2041. [[CrossRef](#)]
12. Durmus, Y.E.; Zhang, H.; Baakes, F.; Desmaizieres, G.; Hayun, H.; Yang, L.; Kolek, M.; Küpers, V.; Janek, J.; Mandler, D.; et al. Side by Side Battery Technologies with Lithium-Ion Based Batteries. *Adv. Energy Mater.* **2020**, *10*, 2000089. [[CrossRef](#)]
13. Nazir, M.H.; Rahil, A.; Partenie, E.; Bowkett, M.; Khan, Z.A.; Hussain, M.M.; Zaidi, S.Z.J. Comparison of Lithium-ion Battery Cell Technologies Applied in the Regenerative Braking System. *Battery Energy* **2022**, *1*, 20220022. [[CrossRef](#)]
14. Uddin, K.; Jackson, T.; Widanage, W.D.; Chouchelamane, G.H.; Jennings, P.; Marco, J. On the Possibility of Extending the Lifetime of Lithium-Ion Batteries through Optimal V2G Facilitated by an Integrated Vehicle and Smart-Grid System. *Energy* **2017**, *133*, 710–722. [[CrossRef](#)]
15. Shariff, S.M. A state-of-the-art review on the impact of fast EV charging on the utility sector. *Energy Storage* **2022**, *4*, e300. [[CrossRef](#)]
16. Banerji, A.; Sharma, K.; Singh, R. Integrating Renewable Energy and Electric Vehicle Systems into Power Grid: Benefits and Challenges. In Proceedings of the 2021 Innovations in Power and Advanced Computing Technologies (i-PACT), Kuala Lumpur, Malaysia, 27–29 November 2021.
17. Nour, M.; Chaves-Ávila, J.P.; Magdy, G.; Sánchez-Mirallas, Á. Review of Positive and Negative Impacts of Electric Vehicles Charging on Electric Power Systems. *Energies* **2020**, *13*, 4675. [[CrossRef](#)]
18. Nazari-Heris, M.; Abapour, M.; Mohammadi-Ivatloo, B. An Updated Review and Outlook on Electric Vehicle Aggregators in Electric Energy Networks. *Sustainability* **2022**, *14*, 15747. [[CrossRef](#)]
19. Ahmadian, A.; Ponnambalam, K.; Almansoori, A.; Elkamel, A. Optimal Management of a Virtual Power Plant Consisting of Renewable Energy Resources and Electric Vehicles Using Mixed-Integer Linear Programming and Deep Learning. *Energies* **2023**, *16*, 1000. [[CrossRef](#)]
20. Lemeski, A.T.; Ebrahimi, R.; Zakariazadeh, A. Optimal Decentralized Coordinated Operation of Electric Vehicle Aggregators Enabling Vehicle to Grid Option Using Distributed Algorithm. *J. Energy Storage* **2022**, *54*, 105213. [[CrossRef](#)]
21. Zheng, Y.; Shao, Z.; Lei, X.; Shi, Y.; Jian, L. The Economic Analysis of Electric Vehicle Aggregators Participating in Energy and Regulation Markets Considering Battery Degradation. *J. Energy Storage* **2022**, *45*, 103770. [[CrossRef](#)]
22. Wu, H.; Shahidehpour, M.; Alabdulwahab, A.; Abusorrah, A. A Game Theoretic Approach to Risk-Based Optimal Bidding Strategies for Electric Vehicle Aggregators in Electricity Markets with Variable Wind Energy Resources. *IEEE Trans. Sustain. Energy* **2016**, *7*, 374–385. [[CrossRef](#)]
23. Thangaraj, A.; Xavier, S.; Ramasamy, P. Optimal Coordinated Operation Scheduling for Electric Vehicle Aggregator and Charging Stations in Integrated Electricity Transportation System Using Hybrid Technique. *Sustain. Cities Soc.* **2022**, *80*, 103768. [[CrossRef](#)]
24. Fathy, A.; Abdelaziz, A.Y. Competition over Resource Optimization Algorithm for Optimal Allocating and Sizing Parking Lots in Radial Distribution Network. *J. Clean. Prod.* **2020**, *264*, 121397. [[CrossRef](#)]
25. Kersch, S.; Arbolea, P. The key role of aggregators in the energy transition under the latest European regulatory framework. *Int. J. Electr. Power Energy Syst.* **2022**, *134*, 107361. [[CrossRef](#)]
26. Lin, H.; Zhou, Y.; Li, Y.; Zheng, H. Aggregator pricing and electric vehicles charging strategy based on a two-layer deep learning model. *Electr. Power Syst. Res.* **2024**, *227*, 109971. [[CrossRef](#)]
27. Alaee, P.; Bems, J.; Anvari-Moghaddam, A. A Review of the Latest Trends in Technical and Economic Aspects of EV Charging Management. *Energies* **2023**, *16*, 3669. [[CrossRef](#)]
28. Wang, Y.; Tian, J.; Sun, Z.; Wang, L.; Xu, R.; Li, M.; Chen, Z. A Comprehensive Review of Battery Modeling and State Estimation Approaches for Advanced Battery Management Systems. *Renew. Sustain. Energy Rev.* **2020**, *131*, 110015. [[CrossRef](#)]
29. Tamilselvi, S.; Gunasundari, S.; Karuppiyah, N.; Razak RK, A.; Madhusudan, S.; Nagarajan, V.M.; Sathish, T.; Shamim, M.Z.M.; Saleel, C.A.; Afzal, A. A Review on Battery Modelling Techniques. *Sustainability* **2021**, *13*, 10042. [[CrossRef](#)]
30. Vardanyan, Y.; Banis, F.; Pourmousavi, S.A.; Madsen, H. Optimal Coordinated Bidding of a Profit-Maximizing EV Aggregator under Uncertainty. In Proceedings of the 2018 IEEE International Energy Conference (ENERGYCON), Limassol, Cyprus, 3–7 June 2018. [[CrossRef](#)]
31. Ma, T.-Y. Two-Stage Battery Recharge Scheduling and Vehicle-Charger Assignment Policy for Dynamic Electric Dial-a-Ride Services. *PLoS ONE* **2021**, *16*, e0251582. [[CrossRef](#)] [[PubMed](#)]
32. Chen, D.; Jing, Z.; Li, Z.; Xu, H.; Ji, T. Exact Relaxation of Complementary Constraints for Optimal Bidding Strategy for Electric Vehicle Aggregators. *Iet Renew. Power Gener.* **2021**, *16*, 2493–2507. [[CrossRef](#)]
33. Najafi, A.; Pourakbari-Kasmaei, M.; Jasiński, M.; Lehtonen, M.; Leonowicz, Z. A Hybrid Decentralized Stochastic-Robust Model for Optimal Coordination of Electric Vehicle Aggregator and Energy Hub Entities. *Appl. Energy* **2021**, *304*, 117708. [[CrossRef](#)]

34. Clairand, J.-M.; González, M.; Cedeño, I.; Escrivá-Escrivá, G. A Charging Station Planning Model Considering Electric Bus Aggregators. *Sustain. Energy Grids Netw.* **2022**, *30*, 100638. [[CrossRef](#)]
35. Simić, M. A Randles circuit parameter estimation of Li-ion batteries with embedded hardware. *IEEE Trans. Instrum. Meas.* **2022**, *71*, 1–12. [[CrossRef](#)]
36. Estaller, J.; Kersten, A.; Kuder, M.; Thiringer, T.; Eckerle, R.; Weyh, T. Overview of Battery Impedance Modeling Including Detailed State-of-the-Art Cylindrical 18650 Lithium-Ion Battery Cell Comparisons. *Energies* **2022**, *15*, 3822. [[CrossRef](#)]
37. Fowler, M.; DaCosta, A.; Mevawalla, A.; Panchal, S.; Fowler, M. Comparative Study of Equivalent Circuit Models Performance in Four Common Lithium-Ion Batteries: LFP, NMC, LMO, NCA. *Batteries* **2021**, *7*, 51. [[CrossRef](#)]
38. Martí-Flores, M.; Cecilia, A.; Costa-Castelló, R. Modelling and Estimation in Lithium-Ion Batteries: A Literature Review. *Energies* **2023**, *16*, 6846. [[CrossRef](#)]
39. Masakure, A.; Gill, A.; Singh, M. The Impact of Battery Charging and Discharging Current Limits on EV Battery Degradation and Safety. In Proceedings of the 2023 3rd Asian Conference on Innovation in Technology (ASIANCON), Pune, India, 25–27 August 2023; IEEE: Piscataway, NJ, USA, 2023; pp. 1–5.
40. Gabbar, H.A.; Othman, A.M.; Abdussami, M.R. Review of Battery Management Systems (BMS) Development and Industrial Standards. *Technologies* **2021**, *9*, 28. [[CrossRef](#)]
41. El Baset Abd El Halim, A.A.; Bayoumi, E.H.E.; El-Khattam, W.; Ibrahim, A.M. Effect of Fast Charging on Lithium-Ion Batteries: A Review. *SAE Int. J. Electrified Veh.* **2023**, *12*, 361–388. [[CrossRef](#)]

Disclaimer/Publisher’s Note: The statements, opinions and data contained in all publications are solely those of the individual author(s) and contributor(s) and not of MDPI and/or the editor(s). MDPI and/or the editor(s) disclaim responsibility for any injury to people or property resulting from any ideas, methods, instructions or products referred to in the content.